IAA-PDC-15-04-19
IMPACT RISK ASSESSMENT AND PLANETARY DEFENSE MISSION PLANNING FOR ASTEROID 2015 PDC

George Vardaxis,[1] Peter Sherman,[2] and Bong Wie[3]
[1]*Corresponding Author, Ph.D. Graduate Student, Asteroid Deflection Research Center, Department of Aerospace Engineering, Iowa State University, Ames, IA 50011, vardaxis@iastate.edu*
[2]*Associate Professor, Iowa State University, shermanp@iastate.edu*
[3]*Vance Coffman Endowed Chair Professor, Iowa State University, bongwie@iastate.edu*

Abstract

In this paper, an integrated utilization of analytic keyhole theory, B-plane mapping, and planetary encounter geometry, augmented by direct numerical simulation, is shown to be useful in determining the impact risk of an asteroid with the Earth on a given encounter, as well as the potential for future encounters. The accurate estimation of the impact probability of hazardous asteroids is extremely important for planetary defense mission planning. Asteroids in Earth resonant orbits are particularly troublesome because of the continuous threat they pose in the future. Based on the trajectories of the asteroid and the Earth, feasible mission trajectories can be found to mitigate the impact threat of hazardous asteroids. In order to try to ensure mission success, trajectories are judged based on initial and final parameters that would make the mission easier to complete. Given the potential of a short-warning time scenario, a disruption mission considered in this paper occurs approximately one year prior to the anticipated impact date. Expanding upon the established theory, a computational method is developed to estimate the impact probability of the hazardous asteroid, in order to assess the likelihood of an event, and then investigate the fragmentation of the asteroid due to a disruption mission and analyze its effects on the current and future encounters of the fragments with Earth. A fictional asteroid, designated as 2015 PDC, is used as a reference target asteroid to demonstrate the effectiveness and applicability of computational tools being developed for impact risk assessment and planetary defense mission planning for a hazardous asteroid or comet.

Keywords: impact risk, impact probability, asteroid 2015 PDC, planetary defense mission

1. Introduction

There is a very real and ever-present threat that Earth faces every day from asteroids. Most of the impacts are from objects that are too small to do any damage on the surface due to the fact that they burn up in the atmosphere. However, there are the rare occurrences where an object does make landfall and causes some serious damage. The number of identified potentially hazardous near-Earth asteroids (NEAs) is increasing, and so too is the likelihood of one of those asteroids posing a non-negligible threat to the planet. The human race is in a unique position to do something about those threats, to either mitigate or eliminate them.

Dealing with the threat of any near-Earth object (NEO) has three main steps: detection/tracking, characterization, and mitigation. NASA, as well as other organizations, have put a lot of effort into the detection/tracking of all near-Earth objects, both threatening and non-threatening. At the Asteroid Deflection Research Center (ADRC) of Iowa State University, there has been a lot of research work done on mitigation methods regarding NEOs with short warning times (<10 years) by studying potential mission designs to disrupt hazardous asteroids. This paper is concerned with asteroid 2015 PDC [1], the disruption mission trajectory design for a Hypervelocity Asteroid Intercept Vehicle (HAIV) to the target body [2, 3], as well as the methodology used to assess the impact risk of an asteroid and its fragments.

An in-house design tool, named as the Asteroid Mission Design Software Tool (AMiDST), is used to conduct the mission and trajectory design for near-Earth asteroid missions [4]. While it does not have the high-fidelity as some of the existing trajectory and mission optimization tools (such as Mystic, MALTO, Copernicus, SNAP,

OTIS, and GMAT), it focuses instead on the launch and terminal phases of the NEO mitigation mission design. AMiDST looks into several launch vehicle and spacecraft configurations based upon several evaluation criteria such as launch vehicle mass capacity and mission ΔV requirements, as well as relative approach velocity and approach angle. In addition to these features, it also provides an estimated total mission cost, used only as a final determination factor between mission configurations.

Techniques such as a high-precision gravitational simulator, encounter geometry, B-plane mapping, and gravitational keyholes are used in this paper to quantitatively evaluate the orbital characteristics of an asteroid and its associated impact risk. A high-fidelity gravitational model is used to propagate the body forward in time to see if and/or when it would come in close proximity to a planet, particularly Earth. These planetary encounters would change the asteroid's orbit, in shape and/or orientation. From the encounter geometry, the post-encounter heliocentric orbit of the asteroid could be in resonance with the planet resulting in another encounter, or potentially an impact. Taking advantage of analytic keyhole theory and the encounter's B-plane, an estimate of the current and future impact probability of the asteroid can be obtained.

A hypothetical impact scenario of fictional asteroid 2015 PDC is considered in this paper. As described in [1], the scenario begins as follows: The asteroid is discovered on April 13, 2015, the first day of the conference, at magnitude 20.9, declination -39 degrees and heading south. It is assigned the designation "2015 PDC" by the Minor Planet Center, and classified as a Potentially Hazardous Asteroid (PHA) based on its orbit. The asteroid's orbital elements are known fairly accurately even in the first few days. Its mean distance from the Sun (semi-major axis) is 1.77 AU, and the orbital eccentricity is 0.49. Its perihelion distance is 0.90 AU and aphelion distance is 2.65 AU; the orbital period is 864 days (2.37 years). The orbital inclination is fairly small: 5.35 deg. The asteroid's orbit comes very close to the Earth's orbit on its outbound leg, much like the Chelyabinsk impactor, but unlike Chelyabinsk, this asteroid impacts at its ascending node. Very little is known about the object's physical properties. Its absolute magnitude is estimated to be about H = 21.3 ± 0.4, which puts the asteroid's size at roughly 100 to 500 meters. The large size uncertainty is due to uncertainties in both albedo and *H* value. At discovery, the asteroid is quite distant from the Earth, about 0.34 AU (51 million kilometers or 32 million miles). It is approaching our planet and slowly brightening, but it peaks at only magnitude 20.3 on May 4. It reaches a closest approach of about 0.19 and it peaks at only magnitude 20.3 on May 4. It reaches a closest approach of about 0.19 AU (28 million km or 18 million miles) from Earth on May 12. It never gets within range of the Goldstone radar and it's too far south at close approach for the Arecibo radar. The JPL Sentry system and University of Pisa's CLOMON system both identify many potential impacts for this object at several future dates. The most likely potential impact date is 2022 Sep 3, but the impact probability for that date is still low in the first week after the asteroid is discovered. Nevertheless, as the object is tracked over the next few weeks, the impact probability for 2022 starts to climb, reaching 0.2% a month after discovery. Even as the asteroid fades past magnitude 22 in early June, it continues to be observed and tracked since the chance of impact just keeps rising. The first part of the scenario ends in mid-June 2015, when the probability of Earth impact in 2022 has reached 1% and continues to rise. The rest of the scenario will be played out at the conference. It is clear that the object will be observable through the rest of 2015, although it will be quite faint (22nd and 23rd magnitude) and observers will require fairly large (2-meter-class) telescopes to track it. In December 2015 and January 2016, the asteroid will fade through 24th and 25th magnitudes, requiring very large aperture telescopes such as the 4- and 8-meter class facilities of CFHT, Keck, Gemini, Subaru, VLT, etc. In the spring of 2016, the asteroid will move too close to the Sun to be observed, and it will remain unobservable for about 7 months. The asteroid's uncertainty region at the time of the potential impact is much longer than the diameter of the Earth, but its width is much less. The intersection of the uncertainty region with the Earth creates the so-called "risk corridor" across the surface of the Earth. The corridor wraps more than halfway around the globe.

2. Asteroid Mission Design Software Tool (AMiDST)

An in-house mission design tool, called AMiDST, is used to conduct the mission and trajectory design for NEO mitigation missions.

2.1. AMiDST Components

In order to run the AMiDST program, the user must input the type of spacecraft that will be used to conduct the mission. The user has two possible spacecraft configurations, a single-body kinetic impactor and a two-body HAIV spacecraft. The desire to use a spacecraft concept like the HAIV comes from the fact that most direct intercept mission with a short warning time (< 10 years) will result in relative arrival velocities of 10 to 30 km/s. The current nuclear subsurface penetrator technology limits the impact velocity to less than about 300 m/s, due to the fact that higher impact speeds prematurely destroy the fusing mechanisms of the nuclear explosive devices (NEDs) [5, 6]. The HAIV concept was developed in order to overcome these technological limitations. As
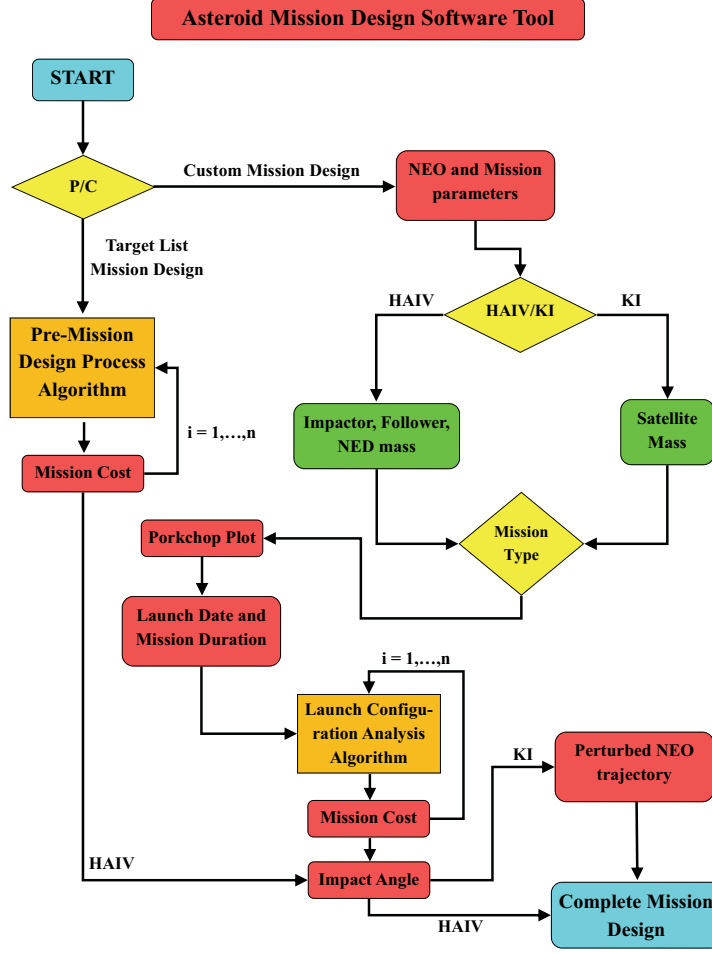
Figure 1: Flowchart Illustration of the AMiDST.

previously mentioned, the HAIV is a two-body spacecraft that consists of a fore-body (leader) and an aft-body (follower), as illustrated in Figures 2 and 3.

Mission cost estimation to design and fabricate the missions is an important task necessary for early assessment of mission viability and feasibility. The final total cost of each mission is given as a combination of the cost for the launch vehicle, the spacecraft, and estimated mission operations. A cost estimation algorithm was developed to determine the costs associated with constructing the spacecraft, based on a number of previous spacecraft missions with similar goals and parameters. Spacecraft such as Deep Impact, Stardust, and Dawn were researched to find the cost of developing such spacecraft and a linear polynomial fit was applied to the data to come up with an analytic formula relating spacecraft mass and cost. As a comparison, the initial mission cost estimates were run through NASA's Advanced Mission Cost Model (AMCM) [7], to get a rough order of magnitude approximation. The estimates from the AMCM came out to be rather rough when it comes to estimating the cost of the constructing the HAIV spacecraft, mostly due to the fact that the HAIV designs don't exactly fit into a single mission category from the available choices. However, the estimates did verify that the estimates are in the appropriate cost range.

The entire design space of mission durations and launch dates is analyzed using a customizable cost function according to user defined mission parameters. The potential design variables are

$$\mathbf{X} = [JD, \Delta V, C3, dispersion, duration, v_{arr}, \alpha_{arr}, \alpha_{LOS}, \alpha_{Sun}] \tag{1}$$

where JD represents the Julian date at mission departure, ΔV is the total mission change in velocity required, $C3$ is the associated mission hyperbolic excess energy at departure from Earth's sphere of influence, $dispersion$ is the dispersion time after disruption, $duration$ is the mission duration, v_{arr} is the relative arrival velocity between the asteroid and the spacecraft, α_{arr} is the relative arrival angle between the asteroid and spacecraft at intercept, α_{LOS} is the line-of-sight angle between Earth and the asteroid at the time of intercept, and α_{Sun} is the approach angle of
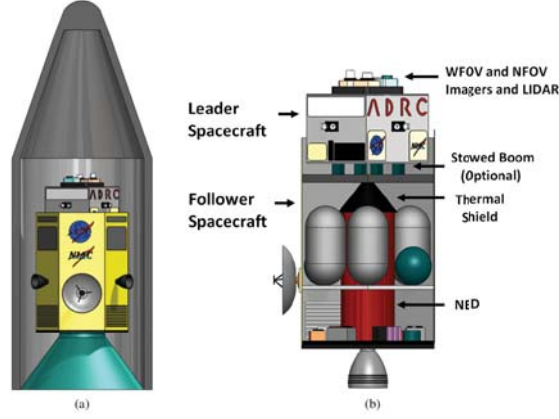
Figure 2: (a) View of the HAIV spacecraft in the payload fairing of a launch vehicle. (b) View of the interior of the HAIV, showing the location of the NED as well as the various spacecraft components[2].
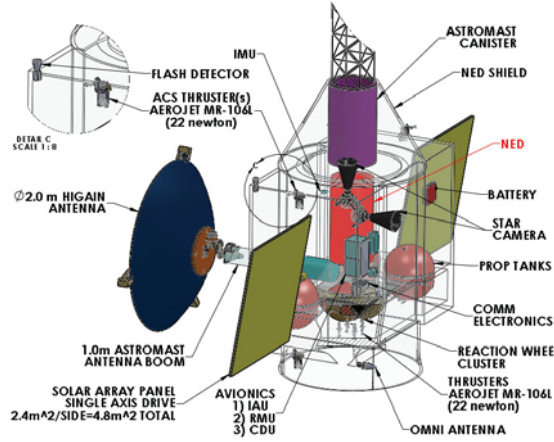

Figure 3: Potential configuration of the HAIV developed by the Mission Design Lab at NASA Goddard Space Flight Center [6].

the spacecraft to the asteroid with respect to the Sun. The cost function is constructed in the following manner

$$C(\mathbf{X}) = f(\mathbf{X}) + g(\mathbf{X}) \tag{2}$$

where $f(\mathbf{X})$ is a constant cost attributed to every mission trajectory and $g(\mathbf{X})$ is a variable cost that is dependent on the state variables used within the trajectory optimization [8]. The components of the overall cost function $f(\mathbf{X})$ and $g(\mathbf{X})$ take the form

$$f(\mathbf{X}) = \Delta V + \sqrt{C3} \tag{3}$$

and

$$g(\mathbf{X}) = g(JD) + g(dispersion) + g(duration) + g(v_{arr}) + g(\alpha_{arr}) + g(\alpha_{LOS}) + g(\alpha_{Sun}) \tag{4}$$

The component cost functions are defined based on the user defined upper and lower bounds for the state variables used in the cost function evaluation of the mission design space.

3. Impact Risk Assessment of Asteroid 2015 PDC

Before any work can be done in regards to rendezvous or disruption mission designs, a certain degree of understanding must be reached in reference to the asteroid's imposed threat to the Earth.

3.1. Propagation Models

The dynamics that govern the motion of a body in space is highly dependent on the model that is used. Within the framework of the work described in this paper, two dynamical models are used: the so-called Standard Dynamical Model (SDM) used to model the free-space propagation of the asteroid body, and a three-body system that incorporates on the effects of the Earth, Moon, and J_2 perturbation for when the asteroid body has passed

4

within the sphere of influence (SOI) of the Earth. Given the short amount of time that the asteroid spends within the Earth SOI, the added perturbations from the Sun and other planets do not amount to enough to warrant their inclusion within the dynamical model used for that system.

The Standard Dynamical Model takes the form [9]

$$\frac{d^2\vec{r}}{dt^2} = -\frac{\mu}{r^3}\vec{r} + \sum_{k=1}^{n}\mu_k\left(\frac{\vec{r}_k - \vec{r}}{|\vec{r}_k - \vec{r}|^3} - \frac{\vec{r}_k}{r_k^3}\right) + \vec{f} \tag{5}$$

where $\mu = GM$ is the gravitational parameter of the Sun, n is the number of perturbing bodies, μ_k and $\vec{r}_k$ are the gravitational parameter and heliocentric position vector of perturbing body k, respectively, and $\vec{f}$ represents other non-conservative orbital perturbation acceleration. The three most well-known are solar radiation pressure (SRP), relativistic effects, and the Yarkovsky effect, the former two being the most prevalent effects. Solar radiation pressure provides a radial outward force on the asteroid body from the interaction of the Sun's photons impacting the asteroid surface. The SRP model is given by

$$\vec{a}_{SRP} = (K)(C_R)\left(\frac{A_R}{M}\right)\left(\frac{L_S}{4\pi c r^3}\right)\vec{r} \tag{6}$$

where $\vec{a}_R$ is the solar radiation pressure acceleration vector, C_R is the coefficient for solar radiation, A_R is the cross-sectional area presented to the Sun, M is the mass of the asteroid, K is the fraction of the solar disk visible at the asteroid's location, L_S is the luminosity of the Sun, c is the speed of light, and $\vec{r}$ and r is the distance vector and magnitude of the asteroid from the Sun, respectively. The relativistic effects of the body are included because for many objects, especially those with small semi-major axes and large eccentricities, those effects introduce a non-negligible radial acceleration toward the Sun. One form of the relativistic effect is represented by

$$\vec{a}_R = \frac{k^2}{c^2 r^3}\left[\frac{4k^2\vec{r}}{r} - \left(\dot{\vec{r}}\cdot\dot{\vec{r}}\right)\vec{r} + 4\left(\vec{r}\cdot\dot{\vec{r}}\right)\dot{\vec{r}}\right] \tag{7}$$

where $\vec{a}_R$ is the acceleration vector due to relativistic effects, k is the Gaussian constant, $\vec{r}$ is the position vector of the asteroid, and $\dot{\vec{r}}$ is the velocity vector of the asteroid [10].

Within the Earth's SOI a similar dynamical model is used to that shown in Eq. 5, where the main gravitating body is the Earth instead of the Sun, the Moon is treated as a perturbing body, and $\vec{f}$ is the J_2 perturbation. In the cartesian frame that the propagation would be done in, the J_2 perturbation takes the following form

$$\ddot{x} = -\frac{\mu x}{r^3} + 3c\left(\frac{x}{r^5}\right)\left(1 - \frac{5z^2}{r^2}\right) \tag{8}$$

$$\ddot{y} = -\frac{\mu y}{r^3} + 3c\left(\frac{y}{r^5}\right)\left(1 - \frac{5z^2}{r^2}\right) \tag{9}$$

$$\ddot{z} = -\frac{\mu z}{r^3} + 3c\left(\frac{z}{r^5}\right)\left(1 - \frac{5z^2}{r^2}\right) \tag{10}$$

where $c = J_2\mu R_\oplus^2/2$, $r = \sqrt{x^2 + y^2 + z^2}$, μ is the Earth's gravitational parameter, J_2 the second zonal harmonic, and $R_\oplus$ is the mean Earth's equatorial radius. The coordinate system is initially fixed with the (x, y) plane corresponding to the Earth's equatorial plane [11].

Taking into account the non-gravitational perturbations in the free-space propagation, the error within the system will increase, but their inclusion would be needed in order to maintain consistency with the planetary ephemeris. A more complete dynamical model, for either the free-space propagation or the flyby propagation, will allow the accurate calculation of asteroid impact probabilities and gravitational keyholes, leading to more effective mission designs. The orbit propagation uses a variable stepsize Runge-Kutta Fehlberg (RKF) 7(8) method that takes into account the effects of the Sun, all eight planets, Pluto, the three largest main belt asteroids (Ceres, Pallas, Vesta), Earth's Moon, as well as the option to include solar radiation pressure and relativistic effects.

3.2. Impact Probability Calculation

Without being given an uncertainty regarding the asteroid's state at epoch, it is hard to accurately assess the impact probability of the asteroid body with the Earth. In this section a discussion is presented over the orbital uncertainty given to the asteroid state and the resulting impact probability calculation.
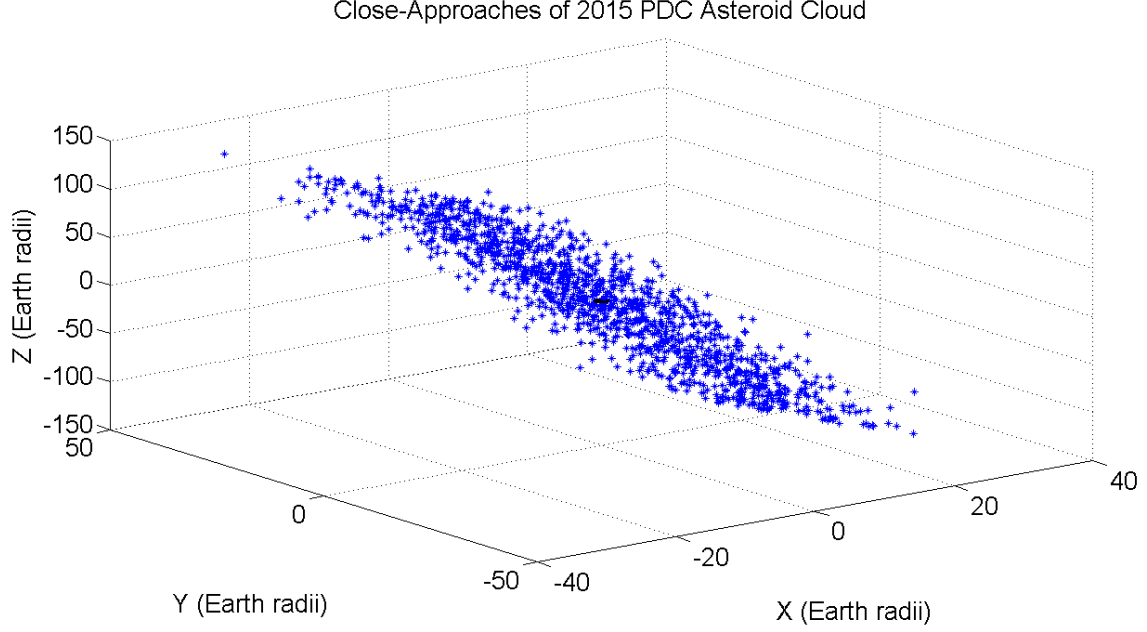
Figure 4: Representation of the virtual asteroid cloud close approaches with initial uncertainties of 50 m and 10 m/s in each coordinate direction, with respect to the Earth's surface.

Table 1: Orbital element covariance matrix for 2,001 virtual asteroid simulation based on normally distributed initial conditions with 50-m position uncertainty and 10-m/s velocity uncertainty

	a	e	i	Ω	ω	θ_0
a	1.018e-06	-6.574e-07	1.436e-06	-8.602e-06	-4.205e-05	5.062e-05
e	-6.574e-07	5.111e-07	-9.148e-07	5.498e-06	1.791e-05	-2.339e-05
i	1.436e-06	-9.148e-07	0.00127	-0.00769	0.00759	7.266e-05
Ω	-8.602e-06	5.498e-06	-0.00769	0.0465	-0.0459	-0.000433
ω	-4.205e-05	1.791e-05	0.00759	-0.0459	0.0487	-0.00308
θ_0	5.062e-05	-2.339e-05	7.266e-05	-0.000433	-0.00308	0.00351

3.2.1. Orbital Uncertainty

Consider an impact risk assessment of the fictional asteroid 2015 PDC. Based on the data provided by NASA's Jet Propulsion Laboratory (JPL), the asteroid's nominal trajectory is known and has an impact probability of about 1%. The uncertainty for the orbit data was not known/given, so certain assumptions are made to find the impact risk of the asteroid. The estimated impact date of asteroid 2015 PDC with Earth is September 3, 2022, based on the nominal trajectory given by JPL. Given that we are mostly interested in the terminal end of the asteroid's trajectory, looking into mitigation strategies that would be needed and implemented about a year before impact, the values reported in this section are based on scenarios where the asteroid is one year from impacting the Earth.

Taking the state vector of asteroid 2015 PDC from the nominal trajectory on September 2, 2021, and adding a standard deviation error on the position values of 50 meters in all three coordinate directions and 10 m/s in all three directions in the velocity, assuming a normal distribution of each position and velocity about their respective mean, the impact probability possessed by the asteroid is about 0.001% based on trajectories of the nominal case and 2,000 additional virtual asteroids. In fact, only 1,304 of the virtual asteroids of the 2,001 virtual asteroids had an encounter with the Earth. If we only consider the number of virtual asteroids that encounter the Earth in our impact probability computation, then the value increases to about 0.00153%. Figure 4 shows all the close approaches of the encountering virtual asteroids. The sphere placed at the origin of the figure represents the Earth. Due to the wide range of close approaches distances, the Earth appears to be very small in comparison, leading so such a small impact probability.

A standard deviation error of position and velocity provides a good measure of the position and velocity variations. But, the best way to understand how initial conditions vary, not only individually but with each other, as compared to other asteroids is to consider a covariance matrix. Table 1 provides the covariance matrix of the orbital element initial conditions presented previously. In Table 1, a denotes the semi-major axis (in units of AU), e the eccentricity, i the inclination, Ω the longitude of the ascending node, ω the argument of periapse, and
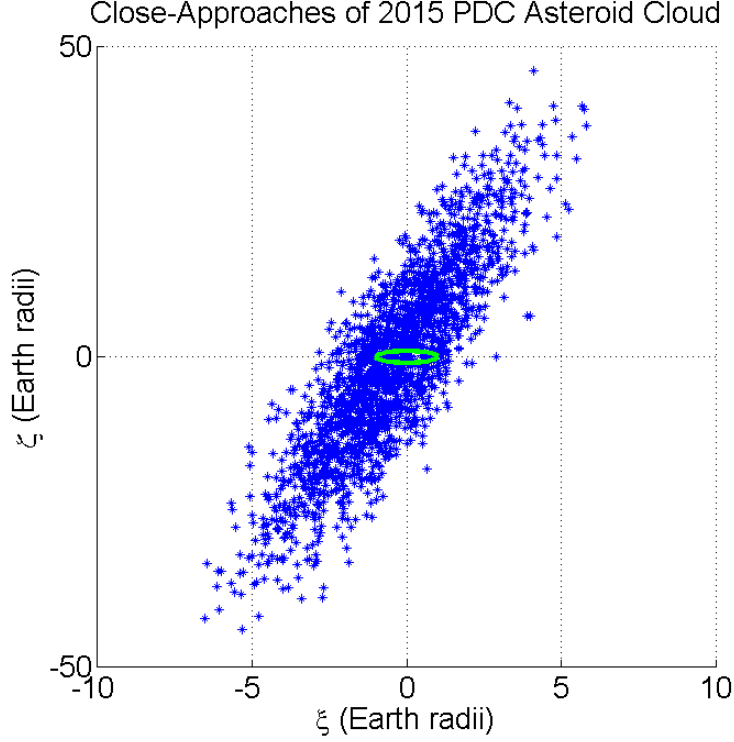
Figure 5: Representation of the virtual asteroid cloud close approaches with initial uncertainties of 50 m and 1 m/s in each coordinate direction, with respect to the Earth's surface.

Table 2: Orbital element covariance matrix for 2,001 virtual asteroid simulation based on normally distributed initial conditions with 50-m position uncertainty and 1-m/s velocity uncertainty

	a	e	i	Ω	ω	θ_0
a	1.0183e-08	-6.574e-09	1.434e-08	-8.662e-08	-4.198e-07	5.061e-07
e	-6.574e-09	5.111e-09	-9.146e-09	5.525e-08	1.788e-07	-2.338e-07
i	1.434e-08	-9.146e-09	1.273e-05	-7.696e-05	7.590e-05	7.248e-07
Ω	-8.662e-08	5.525e-08	-7.696e-05	0.000465	-0.000459	-4.376e-06
ω	-4.198e-07	1.788e-07	7.590e-05	-0.000459	0.000488	-3.073e-05
θ_0	5.061e-07	-2.338e-07	7.248e-07	-4.376e-06	-3.073e-05	3.509e-05

θ_0 the true anomaly angle at epoch - all the angles are in units of degrees. It can be seen in Table 1 that while there is fairly little variation in semi-major axis and eccentricity, the inclination and all the angles that define the orbit's orientation and the position of the body in the orbit have rather large variance and covariance values. In comparison to other near-Earth asteroids, the covariance matrix for 2015 PDC in this scenario is too large to be realistic for such an asteroid.

If we narrow the velocity component variations from 10 m/s to 1 m/s, with the same position component variations and epoch, it is found that all 2,001 of the virtual asteroids cross the Earth's SOI and have an encounter with the Earth. The various depths of encounter for the virtual asteroid cloud can be seen in Figure 5. The impact probability for 2015 PDC, given these position and velocity uncertainties, comes to be about 3.05%. Looking again at the initial orbital element covariance matrix for this asteroid cloud it can be seen that the values in the covariance matrix have all decreased by about two orders of magnitude. This implies that changing the variation in the velocity components by an order of magnitude causes a change in the orbital element covariance matrix as a whole. While all the virtual asteroids have an encounter with Earth and the impact probability has gone up drastically, the covariance is still larger than most near-Earth asteroids that have had several observations by Earth stations or satellites.

If 25 random asteroids (near-Earth asteroids included) are chosen and their covariance matrices are averaged, the corresponding position and velocity variations for asteroid 2015 PDC can be found so that a more accurate impact probability can be found at the given epoch. The asteroids used to compute an average asteroid covariance matrix to compare to that of asteroid 2015 PDC, were asteroids with semi-major axes that were between 1 and

Table 3: Average orbital element covariance matrix for 25 randomly selected asteroids

	e	q	t_p	Ω	ω	i
e	3.240e-08	-4.014e-09	4.279e-07	5.105e-08	8.903e-09	9.819e-07
q	-4.014e-09	2.195e-09	-1.457e-07	1.788e-08	4.620e-08	-7.914e-08
t_p	4.279e-07	-1.457e-07	6.674e-05	-1.267e-06	3.396e-05	1.586e-05
Ω	5.105e-08	1.788e-08	-1.267e-06	6.571e-07	-5.703e-07	1.399e-06
ω	8.903e-09	4.620e-08	3.396e-05	-5.703e-07	3.044e-05	9.181e-06
i	9.819e-07	-7.914e-08	1.586e-05	1.399e-06	9.181e-06	3.503e-05

Table 4: Orbital element covariance matrix for 2,001 virtual asteroid simulation based on normally distributed initial conditions with 1-m position uncertainty and 5-cm/s velocity uncertainty

	a	e	i	Ω	ω	θ_0
a	2.546e-11	-1.643e-11	3.585e-11	-2.167e-10	-1.049e-09	1.265e-09
e	-1.643e-11	1.278e-11	-2.286e-11	1.382e-10	4.470e-10	-5.846e-10
i	3.585e-11	-2.286e-11	3.183e-08	-1.924e-07	1.897e-07	1.8116e-09
Ω	-2.167e-10	1.382e-10	-1.924e-07	1.163e-06	-1.147e-06	-1.095e-08
ω	-1.049e-09	4.470e-10	1.897e-07	-1.147e-06	1.219e-06	-7.681e-08
θ_0	1.265e-09	-5.846e-10	1.812e-09	-1.095e-08	-7.681e-08	8.771e-08

1.5 AU. Some of the notable asteroids that were selected to be apart of the sample were Apophis, Bennu, and 2011 AG5, the rest of the 25 asteroids were selected randomly using the previously mentioned semi-major axis criterion. The average orbital element covariance matrix of the 25 sample asteroids is shown in Table 3 where t_p is the time of periapse given as a Julian Date and q is the perihelion distance in AU. Comparing a few of the values in Table 3 with those in Table 2, it can be seen that while the inclination, eccentricity, and argument of periapse variances are comparable, the variances of the longitude of the ascending node are orders of magnitude different.

As a final check of the impact risk of asteroid 2015 PDC, another 2,001 virtual asteroid simulation was run using the same epoch, but with position uncertainties of one meter in all three directions and velocity uncertainties of five centimeters per second in all three directions. Such small uncertainties brings the initial orbital element covariance matrix of 2015 PDC, much closer to that of the average asteroid for certain parameters and others are shown to be much smaller than their average asteroid counterpart, as shown in Table 4. The smaller orbital element variances that come from such small state vector uncertainties implies that the orbit is more well-defined at this late stage in its trajectory, which would make sense given that it is a year from potentially impacting the planet. In fact, in this scenario asteroid 2015 PDC has about a 57% chance of impacting the Earth. If the impact probability is this high at the given point in time, the only chance that humanity would have to avoid getting hit by the whole asteroid would be to fragment the body and give the fragments time to disperse over the asteroid's orbital path, and would only have to run the risk of having a small fraction of the asteroid mass encounter the Earth.

4. Impact and Keyhole Passage Risk Assessment

This section provides a discussion of the methods employed to assess the possibility of an asteroid or asteroid fragment impacting the Earth or passing through a gravitational keyhole to impact the planet at a future date.

4.1. Impact Risk Assessment

One of the simplest ways, in theory not necessarily computationally, of calculating an impact probability of an asteroid and a planet is to simply construct a fiels of virtual asteroids about the reference trajectory of the asteroid, propagate them all through the anticipated encounter date, and calculate the impact probability by dividing the number of virtual asteroids that hit the planet, known as virtual impactors, by the total number of virtual asteroids used in the computation. A drawback of this method is that it can be computationally expensive, and the number of virtual asteroids that would need to be used needs to be at least equal to the inverse of the impact probability [14]. Alternative methods of impact probability computation have been developed in the literature by using an impact probability model of the form

$$IP = \int \int \int_{V_\oplus} PDF(x, y, z)dxdydz \qquad (11)$$

To simplify the calculation, the three-dimensional PDF can simplified to one-dimensional by converting the (x, y, z) position data to spherical coordinates (r, θ, ϕ), and the triple integral would turn into a single integral over the radius

8

of Earth,

$$IP = \int_0^{r_\oplus} PDF(r)\, dr = CDF(r_\oplus) - CDF(0) \tag{12}$$

where CDF denotes the cumulative density function resulting from the radial PDF. It has been shown previously [4, 16]

$$IP = \frac{1}{2}\left[erf\left(\frac{r_\oplus - \mu}{\sigma\sqrt{2}}\right) - erf\left(\frac{0 - \mu}{\sigma\sqrt{2}}\right)\right] \tag{13}$$

that the difference between the CFD value at zero and at Earth's radius results in a difference in the error function, in terms of the mean (μ) and standard deviation (σ) of the virtual asteroid close-approach radii.

This formulation is incorrect in that analysis however, particularly Equation (13). If the initial variations in (x, y, z) position are normally distributed about their own means and an associated standard deviations, then the the resulting error function stemming from the radial PDF would be incorrect. The probability density function of the error function is a normal distribution, meaning that the radius values of the close-approach values would have to be normally distributed, which is not true given that (x, y, z) are normal and $r = \sqrt{x^2 + y^2 + z^2}$. The radial distribution would be Rayleigh or shifted Rayleigh, using two normally distributed, independent variables (x, y), or even two planar orthogonal coordinates (e.g., (ξ, ζ)). The vector magnitude of the crossing points would be a Rayleigh distribution, assuming the components are uncorrelated with equal variance and zero mean. The crossing data will not necessarily have equal variance or zero mean, so a distribution (some type of gamma distribution possibly) can be fit to the radial position data in order to find a better estimate of the impact probability. The formulation results in a number between 0 and 1, corresponding to the probability of impact. Having a larger pool of virtual asteroids used in the computation increases the computation time, but should yield a more accurate impact prediction.

4.2. Keyhole Passage Risk Assessment

When looking for the possibility of passing through a keyhole on the target B-plane, looking simply at the radial distribution of the data does not distinguish between data points that are in the correct region of the B-plane and those that have the component combinations that would result in the radial distance associated with a keyhole. Different methods exist to answer that question, such as long-term orbital simulations tracking the asteroids or asteroid fragments or analytic keyhole theory to find the regions in an encounter B-plane that would result in a resonant return with the planet. Each method has a cost associated with it, the long-term orbital simulations can take a large amount of computation time but are fairly high-fidelity, while the analytic theory takes a significantly smaller amount of computation time while proving lower-fidelity results.

4.2.1. Area Method for Keyhole Passage Assessment

The virtual fragments constructed through the orbital uncertainty of a single asteroid fragment propagated through the encounter B-plane occupy a fraction of the B-plane's area. The keyhole on the same encounter B-plane also occupies a fraction of the B-plane area, however, not necessarily the same or even overlapping areas of the B-plane. This method claims no accuracy, only that it can be a way to quickly evaluate the risk potential of an asteroid and/or its fragments, and the method does not hold for instances where the keyhole region and the virtual fragment cloud region are too far removed from each other, where the keyhole passage probability would be assumed to be zero.

Consider the case where the keyhole region resides near the virtual fragment cloud of the asteroid fragment: how do we effectively evaluate the potential of the fragment to fall within the keyhole region? This question is answered using an area method that attempts to capture a majority of the virtual fragments within a bounding box and is proportional to the ratio of the area of the keyhole region and the bounding box. The example presented here is only to show the methodology employed, it is not intended to describe an accurate, real-life scenario.

Assume that an asteroid has a virtual asteroid cloud, comprising of 10,000 virtual asteroids, passing through the Earth's encounter B-plane such as that indicated by the blue stars and the red stars showing the position of the same virtual asteroid cloud on the next encounter B-plane in Figure 6. The yellow stars in each cloud indicate the virtual asteroids that pass within 1.1 Earth radii on the second encounter B-plane. It is worth mentioning that the crossing points on the first encounter B-plane were created such that the probability of an impact with the planet on the first pass is zero. Before discussing the first encounter crossing point data, let's look at the second encounter data. Of the 10000 virtual asteroids, 66 fall within 1.1 Earth radii of Earth's surface on that particular encounter, making the impact probability for the encounter 0.66%. Calculating the impact probability using a radial position density function, the resulting impact probability is estimated to be about 0.71%, showing strong agreement between the statistical approximation and the simulated results.

Now, let's look back to the first encounter crossing data, it can be seen that there is a black box and ellipse over the crossing point data. The box is constructed to have dimensions large enough to encompass at least 90%
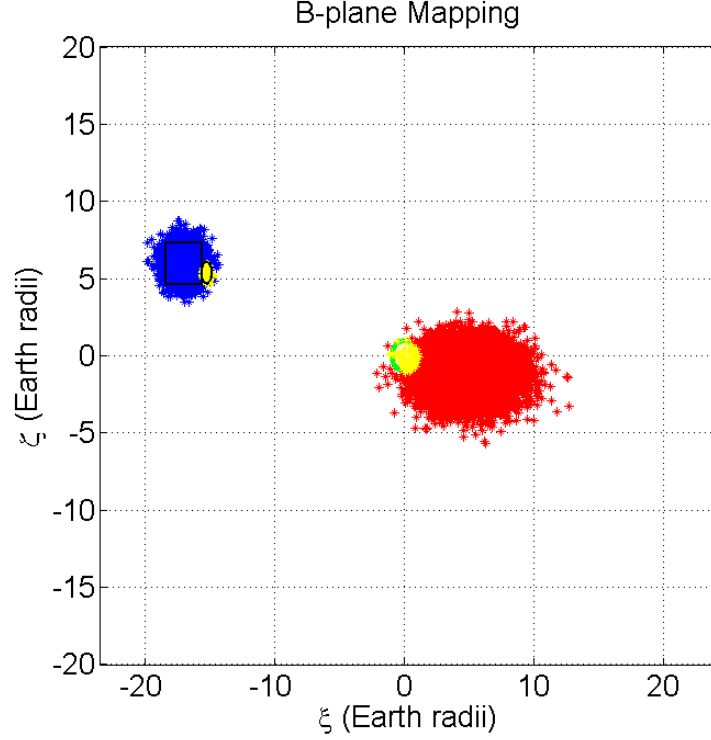
Figure 6: Example composite encounter B-plane for successive encounters of an asteroid with Earth.

of the data points, and the ellipse is constructed with dimensions such that 95% of the data points fall within the prescribed area. The precentage values given are simply chosen to capture a large majority of the crossing points within each region and hold no special significance. When implemented using a simulated asteroid fragment, the dimensions of the keyhole region will be established based on the theory, so the proportion of the crossing points falling within the area will be simply the number within the region divided by the simulated fragments.

So, to construct the impact risk assessment for the asteroid based on its virtual asteroid field

$$IP = \left[\frac{A_{ellipse}}{A_{box}} \right] p_{box} \, p_{ellipse} \, (1 - p_{ellipse}) \qquad (14)$$

where $A_{ellipse}$ and A_{box} are the areas of the ellipse and box encompassed by those shapes on the encounter B-plane, respectively, and p_{box} and $p_{ellipse}$ are the proportion of the crossing points that fall within the box and ellipse, respectively. With the resulting formula, the probability of an impact by the asteroid on its second encounter with Earth is evaluated to be about 0.5%.

Looking at the result, it is easy to see that it is not the same value as those found using either the statistical approximation or the simulated results on the second encounter B-plane crossing data. The results shouldn't be expected to be the same, or even necessarily in the same ballpark, because depending on the amount of time between encounters the field of virtual asteroids can disperse quite a bit leaving the impact probability on the second encounter plane to be essentially zero. As previously stated, this formula is not guaranteeing the accurate assessment of the impact probability of a body on future encounters, but is simply being used to find a solution so as to give an evaluation of whether or not the body would need to be studied further.

So, the expression described by Equation (14) needs to be revised a bit to find the probability of the asteroid/fragment passing through the keyhole on the B-plane. Firstly, the definition of $p_{ellipse}$ needs to be changed. Originally, $p_{ellipse}$ represented the proportion of the virtual cloud on the first encounter B-plane that would impact the Earth on the second encounter B-plane. Now, it represents the proportion of the cloud that falls within the keyhole region because in the case of a simulated asteroid fragment cloud, unless the cloud is simulated through to the second encounter B-plane, the number that would impact the Earth would be unknown and the size of the keyhole on the first encounter B-plane would be known (or at least established). And secondly, in order to deal with the varying potential keyhole locations on the encounter B-planes, a term has to added to the expression to represent the proportion of the cloud that makes an encounter with the Earth after the fragmentation event. The resulting equation used to calculate the probability of an asteroid, or asteroid fragment, passing through a keyhole
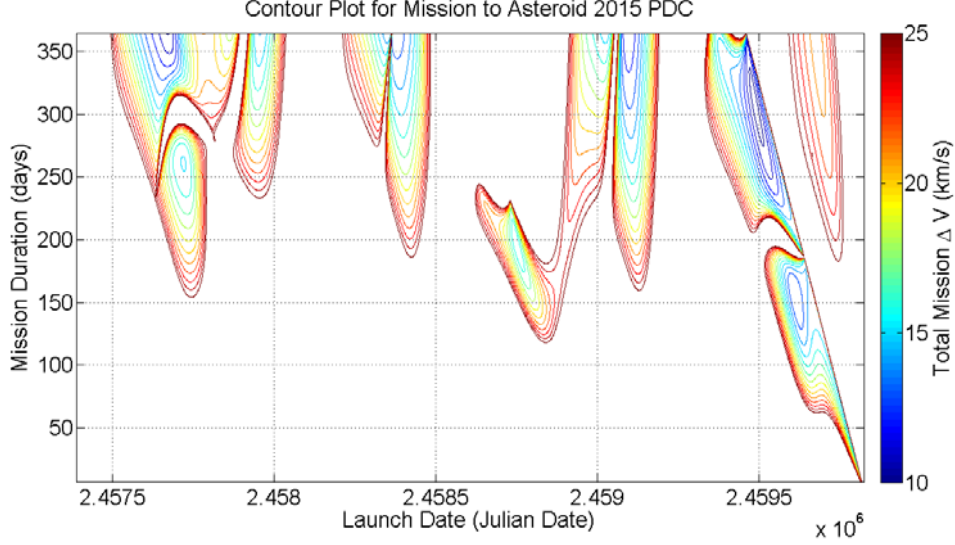
Figure 7: Contour plot of total mission ΔV for a rendezvous mission to asteroid 2015 PDC before its potential Earth impact in 2022.

now takes the form

$$KP = p_{encounter} \left[\frac{A_{ellipse}}{A_{box}} \right] p_{box}\, p_{ellipse}\, (1 - p_{ellipse}) \tag{15}$$

where $p_{encounter}$ is the proportion of the asteroid/fragment cloud that encounters the Earth, $A_{ellipse}$ is the area of the ellipse that represents the keyhole region of the B-plane, A_{box} is the area of the bounding box that encompasses a sizable portion of the virtual cloud, p_{box} is the proportion of the cloud that is encompassed by the bounding box, and $p_{ellipse}$ is the proportion of the virtual cloud that falls within the elliptical representation of the keyhole.

If the keyhole exists in a high density region of the virtual cloud, then the resulting keyhole passage probability from Equation (15) is representative based on the population. A problem arises when the keyhole falls in a low density region of the virtual cloud. In the case where a handful or so of the virtual asteroids/fragments fall into or near the keyhole region, the keyhole passage probability can drop dramatically. So something to keep in mind when looking at the resulting probability values from Equation (15) is the spread of the data and if the number of data points used is sufficiently large to accept the reported answer. A study could be done to find the number of sufficient bodies, which is not done within this work's scope.

5. Mission Designs for Asteroid 2015 PDC

The fictional asteroid 2015 PDC is detected on April 13, 2015 and is believed/known to be on an Earth-impacting trajectory, with a predicted impact on September 3, 2022. That means that there is about seven years of time in which any missions can be devised and conducted for reconnaissance or deflection/disruption attempts. Since the asteroid is only estimated to have a 0.2% impact probability shortly after its discovery, a rendezvous mission to the target body is considered in order to gain more information about the asteroid's orbit and physical parameters. Once a rendezvous mission has launched and had some time near the target, a disruption mission to the hazardous body can be launched to try and mitigate the threat to Earth.

5.0.2. Rendezvous Mission Designs

For a rendezvous mission, one of the most important parameters to consider, beyond the ability to place the spacecraft into the appropriate trajectory to meet the target, is the speed at which the spacecraft approaches the target. The spacecraft has long since detached itself from the launch vehicle that placed it into its interplanetary trajectory, so the velocity difference between the spacecraft and the target body is the spacecraft's responsibility to make up. If that speed is too large, the spacecraft would require a large amount of propellant in order to make up the speed difference, which in turn may require a larger launch vehicle to place the spacecraft into orbit. Therefore, one of the quantities to be minimized through the mission optimization process is the total mission ΔV. Figure 7 shows the resulting rendezvous mission contour plot for asteroid 2015 PDC. Looking at the contour plot, it is easy to see that there are only a handful of regions where potentially feasible rendezvous missions could exist to this asteroid body. Most of the potentially mission feasible regions lie at the top of the contour plot, where the mission durations are highest. There is one region however that could have feasible missions around 150 days
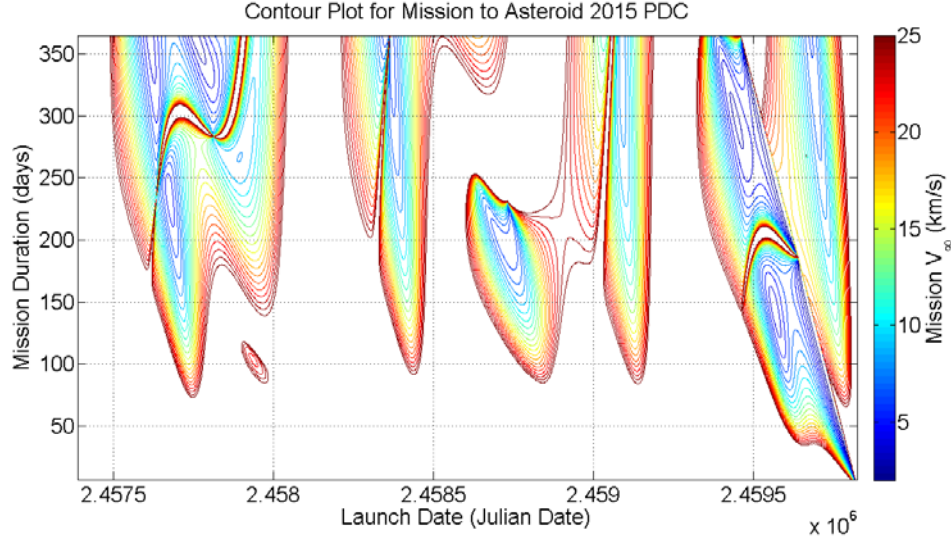
Figure 8: Contour plot of mission V_∞ for a rendezvous mission to asteroid 2015 PDC before its potential Earth impact in 2022.

in duration, but the launch date is about a year prior to the expected impact date. Such a late launch date for a rendezvous, reconnaissance mission does not really allow for the potential of several deflection/disruption mission attempts, in the case that they fail or do not have the desired effect. In order to allow for a larger window in which deflection/disruption missions can be conducted in, the time between target acquisition and the expected impact date, within the AMiDST program, will have a lower bound limit of 1000 days (about 3 years).

Total mission ΔV and acquisition time are only two of the important mission parameters needed to evaluate mission logistics, the mission V_∞ is also needed in order to assess the relative ease with which the launch vehicle can set the spacecraft in its interplanetary orbit. A lower mission V_∞ would indicate that the interplanetary orbit would be easy to enter into, after leaving the Earth's sphere of influence. On the other hand, a higher mission V_∞ would be either because the energy of the hyperbolic orbit needed to enter into the required interplanetary trajectory is very large or the interplanetary trajectory is out of the ecliptic plane. Figure 8 shows the rendezvous mission V_∞ contour plot for asteroid 2015 PDC. Observing the contour plot, it can be seen that the low mission V_∞ values exist in the same regions as the low mission ΔV values, and in a couple other regions as well. In those regions where the V_∞ values are low and the ΔV values are not, it would imply that the relative arrival velocity between the spacecraft and the target body is the larger contributor to the overall mission ΔV. Despite the requirement and limitations placed on the value of the mission V_∞, in regards to the optimal rendezvous mission, the limiting factor in this particular mission design will be the total mission ΔV and the relative arrival speed.

In order to find the optimal rendezvous mission for a spacecraft mission to asteroid 2015 PDC, the following mission parameters were chosen as a part of the optimization process: launch date, total mission ΔV, mission $C3$, target acquisition time, mission duration, and relative arrival speed. The resulting mission trajectory is shown in Figure 9. The green line indicates the track that Earth takes during the time that it takes the spacecraft (blue line) to arrive at asteroid 2015 PDC (red line). Within the time that it would take the Earth to complete one revolution, the spacecraft launched on September 5, 2018 would arrive at asteroid 2015 PDC and begin its reconnaissance mission. The launch window surrounding this optimal mission is fairly small, about four days in length. Despite the limited length of the launch window, the remaining of the top ten missions occur within that same launch window but with varying length of mission durations. From that optimal launch window, there would be around 1094 days between the spacecraft's encounter of the asteroid body and the expected impact date for the spacecraft to observe the physical parameters of the body and trackle the asteroid's orbit track around the Sun.

Based on the shape of the spacecraft trajectory for the optimal rendezvous mission depicted in Figure 9, the spacecraft has to be launched from Earth's sphere of influence on a fairly high energy hyperbolic orbit ($C3 \approx 26.5$ km^2/s^2) because while the interplanetary orbit stays near the Earth's ecliptic plane, the trajectory reaches beyond Mars orbit and encounters the asteroid body nearly 2 AU from the Sun (almost 3 AU from Earth). The total mission ΔV is about 12.38 km/s, about 8 km/s of which are needed by the spacecraft to match the asteroid's speed. Based on the resulting optimal rendezvous mission parameter values, the necessary ΔV that the spacecraft needs to match the asteroid's speed is relatively large - meaning that the spacecraft needs to be large enough to hold the necessary fuel needed to make that change in speed. In fact, about 85% of the total spacecraft mass would need to be fuel in order to successfully achieve that kind of velocity change. So, if the largest version of the HAIV
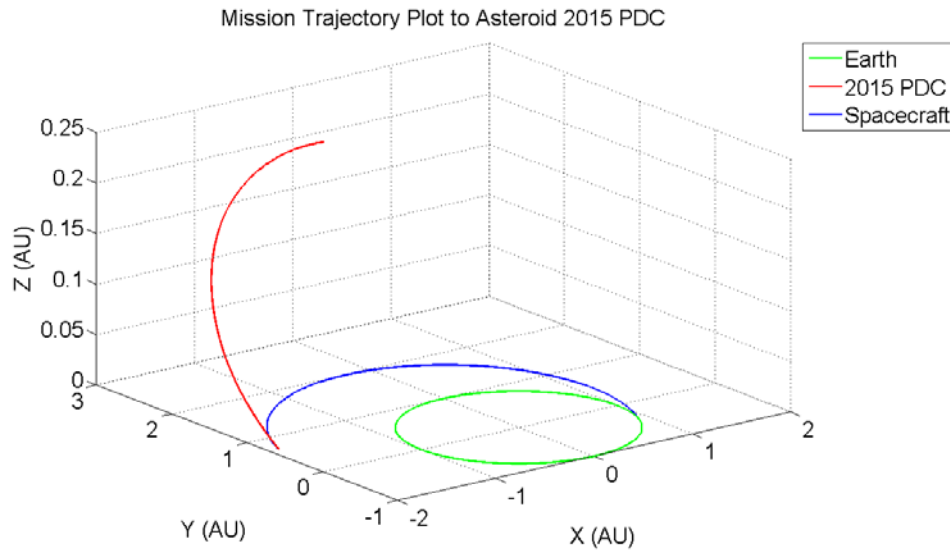
Figure 9: Trajectory plot for the optimal rendezvous mission to asteroid 2015 PDC between its discovery date and the expected impact date.

spacecraft is chosen to carry out this mission (mass of 5,720 kg), then only about 950 kg of the spacecraft mass would be available to be used for the payload, structure, and instrument suites. Assuming that a large enough spacecraft was constructed, capable of performing the speed matching maneuver, the mass of the spacecraft and the energetic orbit that it would have be placed in to reach its target in the time alloted would imply that a large launch vehicle is needed to place that spacecraft into the corresponding interplanetary orbit - large Delta IV or Atlas V class launch vehicle. To ensure mission success, a large Atlas V or Delta IV launch vehicle, such as the Atlas V 551 or Delta IV Heavy, is chosen to be used to complete this optimized rendezvous mission. The total cost to construct the spacecraft, launch vehicle, and conduct the mission operations for this optimized rendezvous mission would be over $2.1 billion. If the situation truly warranted a rendezvous mission that would enhance the knowledge of a potentially hazardous near-Earth asteroid, the total mission cost would not be the determining factor but be considered a small price to pay for future Earth safety.

5.1. Disruption Mission Designs

The difference between a disruption mission and a rendezvous mission is the approach to the target body. Through the use of the HAIV spacecraft, the relative arrival speed between the spacecraft and the target asteroid body is necessary to be known for the timing sequence between the fore and aft bodies, but is fairly inconsequential as far as the optimization is concerned. The optimization process would be conducted in much the same way, but would ignore the relative arrival speed of the spacecraft to the target asteroid. Before looking at the different mission design types ((1) long-duration, long-dispersion, (2) long-duration, short-dispersion, (3) short-duration, long-dispersion, and (4) short-duration, short-dispersion), the total mission ΔV (Figure 10) and V_∞ (Figure 11) contours can be analyzed to understand how accessible asteroid 2015 PDC is from Earth between 2015 and 2022 for an disruption mission. Examining Figure 10, it can be seen that short-durations missions (less than 100 days) would be very difficult to be feasibly constructed for a spacecraft, outside a few months before the expected impact date. When looking at mission durations of more than 100 days, it appears that there are periodic regions of the contour plot where a an intercept mission can be launched to asteroid 2015 PDC. The V_∞ contour in Figure 11 validates the notion that short-duration missions would be hard to come by before the few months prior to the expected impact. Observing the remaining portion of Figure 11, it can be seen that the accessible regions of the contour plot are smaller than what they appeared to be in ΔV contour plot. Based on the V_∞ contour plot, the easiest times to launch a mission would be soon after its discovery (around the 2015/2016 time frame) and within a year of the anticipated impact date. Due to the lateness of the rendezvous mission's departure date and the focus of the studies conducted by the ADRC being oriented about short-warning times, the mission types that will be looked at will be long-duration, short-dispersion and short-duration, short-dispersion mission designs. The rendezvous mission arrives at the target body nearly three years prior to the expected impact date, but to give time for the spacecraft to gather enough information about the orbit and the physical characteristics of the asteroid, the mission designs discussed here will focus on dispersion times between seven and 90 days in length - true last minute disruption missions.
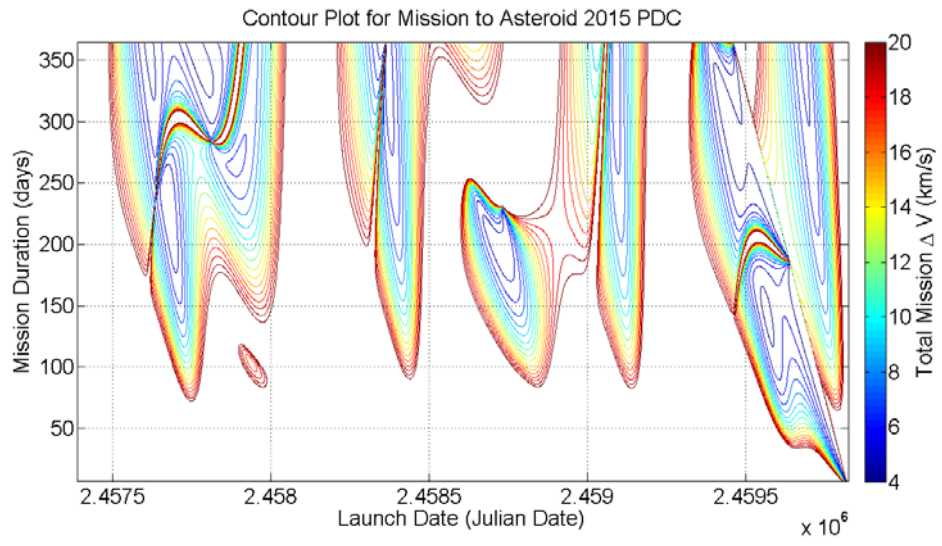
Figure 10: Contour plot of total mission ΔV for an intercept mission to asteroid 2015 PDC before its potential Earth impact in 2022.
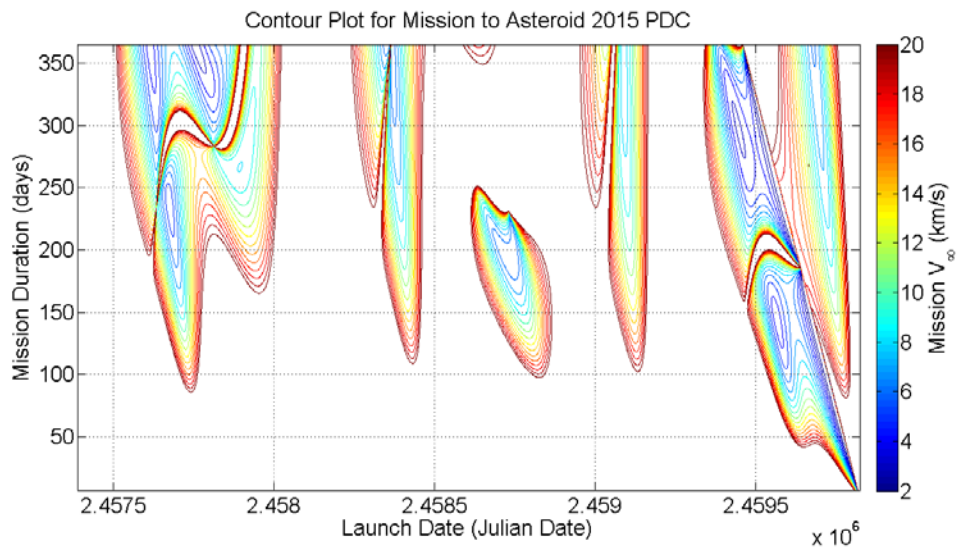

Figure 11: Contour plot of mission V_∞ for an intercept mission to asteroid 2015 PDC before its potential Earth impact in 2022.
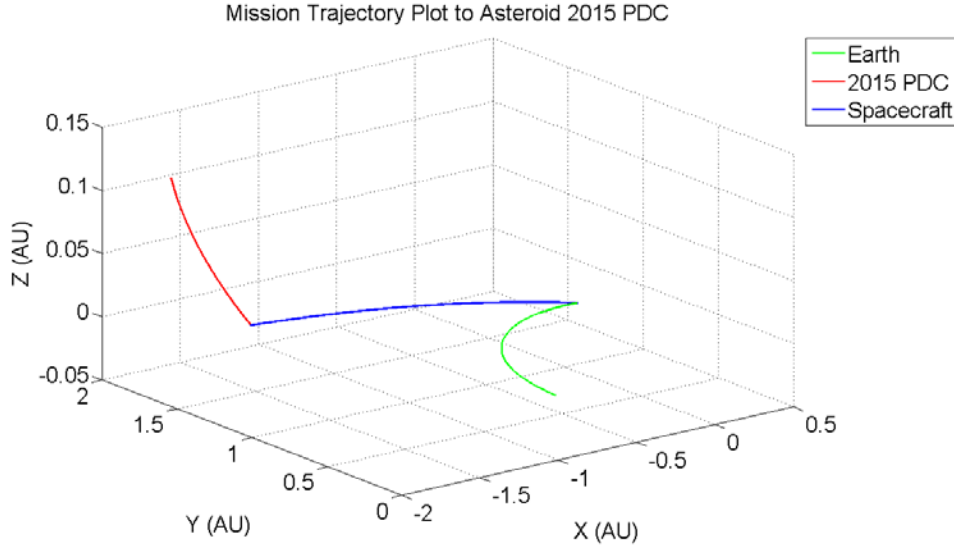
14

Figure 12: Trajectory plot for a short-duration, long-dispersion intercept mission to asteroid 2015 PDC.

5.1.1. Short-duration, Long-dispersion Mission

As already stated, the ability to conduct a feasible short-duration, long-dispersion mission is not practical. However, this mission type is the most desirable disruption mission type given its tendency to maximize the amount of time from launch to the anticipated impact date. For the case of asteroid 2015 PDC, the optimal short-duration, long-dispersion mission results are discussed here briefly to show its impracticality.

The required mission ΔV and $C3$ orbit for a short-duration, long-dispersion mission scenario would be too large for any launch vehicle currently in operation to place even a small spacecraft into the necessary orbit to intercept the target body. None of the top 10 optimal missions are feasible: the mission ΔV is nearly 14 km/s from LEO and the required orbit $C3$ is about 350 km^2/s^2. The trajectory depicted in Figure 12, gives justification for the highly energetic orbit required by the spacecraft to leave Earth and meet 2015 PDC. The optimization process tried to push the mission duration as high as possible, in an attempt to reduce the required ΔV and $C3$, but the restriction of a maximum mission duration of 90 days did not allow for more feasible missions to be considered in this analysis. The date at which this short-duration, long-dispersion mission would launch would be in the middle of a launch window centered on December 18, 2016, a little more than a year and a half after discovery of asteroid 2015 PDC. To compound the difficulty of this mission design, if there was some way of getting the spacecraft into the required interplanetary orbit, there would be the added difficulty of the hypervelocity encounter between the spacecraft and asteroid. In the case of this optimal mission design, the relative arrival speed between the two bodies comes to be about 35 km/s, much faster than any relative arrival speed found in other optimal mission designs. It is possible that a more feasible optimal mission design could be obtained with an alternate definition of short-duration, but for the sake of consistency between this example asteroid, and the other asteroids studied [4], the definition is unaltered.

5.1.2. Long-duration, Short-dispersion Mission

Trying to keep the mission duration as long as possible should reduce the necessary amount of mission ΔV needed to get into the required orbit. The resulting optimal long-duration, short-dispersion mission results in a total ΔV requirement of 3.273 km/s, most of which would be provided by the launch vehicle leaving from LEO, and a mission $C3$ of about 1 km^2/s^2. And with a spacecraft mass of about 2,500 kg, this mission is easily feasible for most any launch vehicle to accomplish. The top mission trajectory to asteroid 2015 PDC does not deviate from the ecliptic much and doesn't need to go far outside the Earth's vicinity, which explains the small $C3$ value and is made evident by Figure 13. The optimization algorithm was allowed to evaluate missions with durations between 200 and 365 days, where the dispersion time after the spacecraft encounters the target asteroid can be between 7 and 90 days. The top resulting mission design had a mission duration of 245 days and a dispersion time of 7 days. In fact, this mission was in the middle of a 10 day launch window of optimal missions, where all optimal missions had dispersion times of 7 days, despite the allowance for more time, and the variation in launch date resulted in a corresponding change to the mission duration. The length of the mission duration and launch date correspond to the short dispersion time, and with an expected spacecraft encounter one week prior to Earth impact, the relative arrival speed between the spacecraft and the asteroid is understandably over 10 km/s, meaning that the guidance
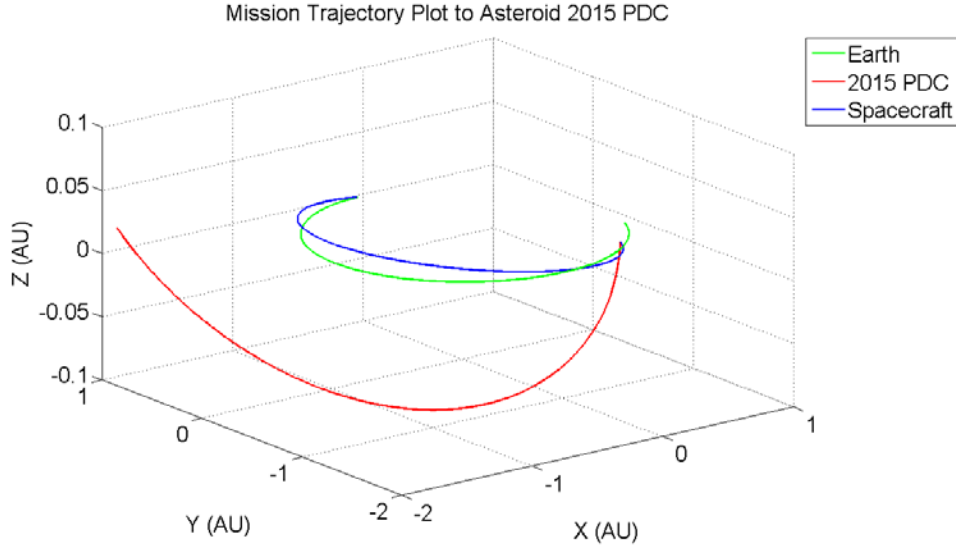
15

Mission Trajectory Plot to Asteroid 2015 PDC

Figure 13: Trajectory plot for a long-duration, short-dispersion intercept mission to asteroid 2015 PDC.

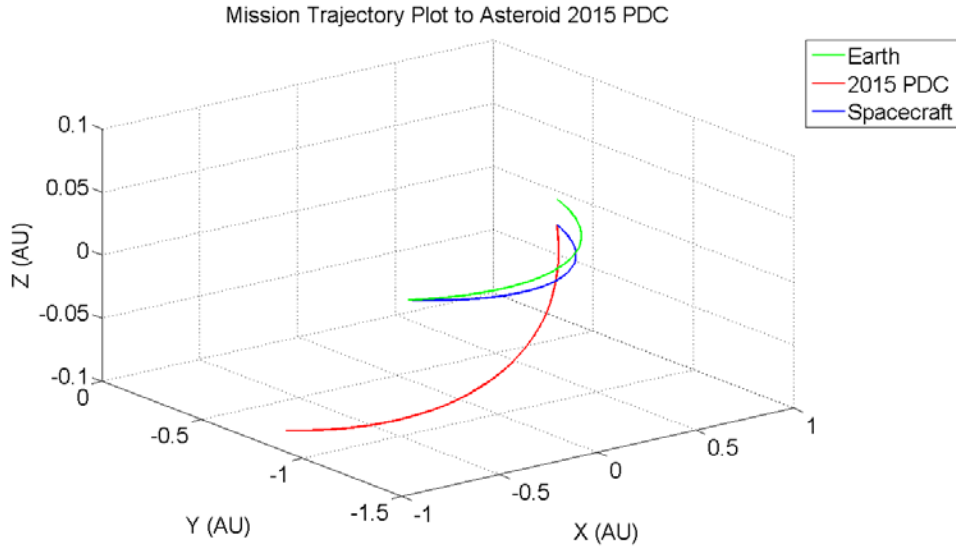Mission Trajectory Plot to Asteroid 2015 PDC

Figure 14: Trajectory plot for a short-duration, short-dispersion intercept mission to asteroid 2015 PDC.

algorithms would need to be fast-responding and highly precise because there is no room for failure.

5.1.3. Short-duration, Short-dispersion Mission

Assuming that it is too late for all other options, or even worse they have all failed, to diminish the threat posed by asteroid 2015 PDC, a short-duration, short-dispersion mission design is constructed to deal with the imminent threat from the target asteroid. A short mission duration and short dispersion time implies that the asteroid has now entered the terminal phase of its orbit with respect to the Earth. Thus, with such a late launch window, the task of reaching the asteroid from Earth should be simpler to accomplish. The additional constraint of a short mission duration means that the mission duration has the same time restraint as the dispersion time (7 to 90 days). The optimal mission trajectory, depicted in Figure 14, shows the simplicity of the orbit needed by the spacecraft to leave Earth and intercept the asteroid. The results from optimization process show that the longer the mission duration and the shorter the dispersion time for the desired intercept mission would produce a more manageable design. Low total mission ΔV and $C3$ values allow for larger spacecraft and/or smaller launch vehicles to be used, but the hypervelocity relative arrival speed ($\approx$12 km/s) between the spacecraft and the asteroid mandates the use of a spacecraft similar to the HAIV for any attempted fragmentation mission.

Despite the ease of these types of mission designs, late launch date and short-dispersion time, it should be noted that they should be considered as a last resort when all other attempts have failed, and not considered only
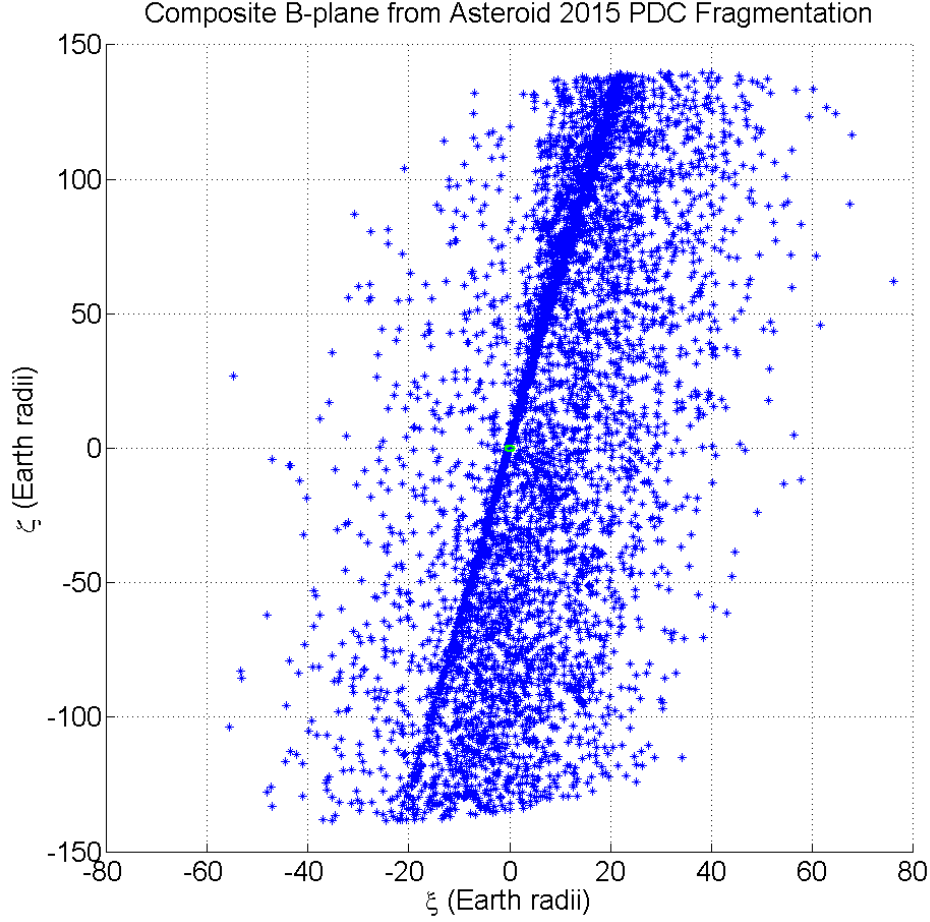
Figure 15: Composite encounter B-plane showing the crossing locations of asteroid 2015 PDC's fragments.

when there are no other options able to be taken.

5.2. Fragmentation of Asteroid 2015 PDC

Because the work conducted by the ADRC focuses on short warning times, the time from the disruption event to the asteroid fragments encountering the planet is set to be one year. Assuming the fragment states are normally distributed about the nominal asteroid trajectory's states, before the radial perturbation is applied to each fragment, the fragments are then propagated over that year time span through to their individual encounters with the Earth. The resulting crossing points of the 10001 virtual asteroid fragments on the encounter B-plane are shown in Figure 15. It can be seen from the composite B-plane that the asteroid fragments are spread across a wide portion of the map. For reference, a small circular cross-section of the Earth can be seen centered at the origin.

Of the numerous simulated fragments of asteroid 2015 PDC, a fragment is selected that crosses the B-plane fairly close to the Earth (about 9 Earth radii from the center of the planet. Using state standard deviations of 10 meters and 1 meter per second, normally distributed about the nominal asteroid fragment states, a field of 10,000 virtual fragments is created and propagated through the encounter B-plane, in addition to the nominal asteroid fragment's trajectory. Figure 16 shows the crossing locations of the virtual fragment field on the encounter B-plane. It can be seen that the 2015 PDC fragment cloud encompasses the Earth. In fact, about 2.9% of the 10,001 simulated virtual fragments pass within 1.1 Earth radii of the center of the planet. A histogram of the radial distances of the fragment cloud crossing positions is shown in Figure 17. The radial position histogram shows a skewed distribution, with a large portion of the data being between 0 and about 12 Earth radii. Fitting a gamma distribution to the radial position data, the calculated probability that the asteroid fragment would fall within 1.1 Earth radii is approximately 2.4%. The B-plane component distributions for the 2015 PDC asteroid fragment appear to be nearly normal. But, as previously stated, it cannot be assumed that just because the initial fragment field states are normally distributed that the resulting B-plane components would be normally distributed. The histograms in Figure 18 show the distributions of the fragment cloud's B-plane components. Looking at the ξ-component, the distribution appears to be pretty normal, with a mean a bit larger than one Earth radius. The
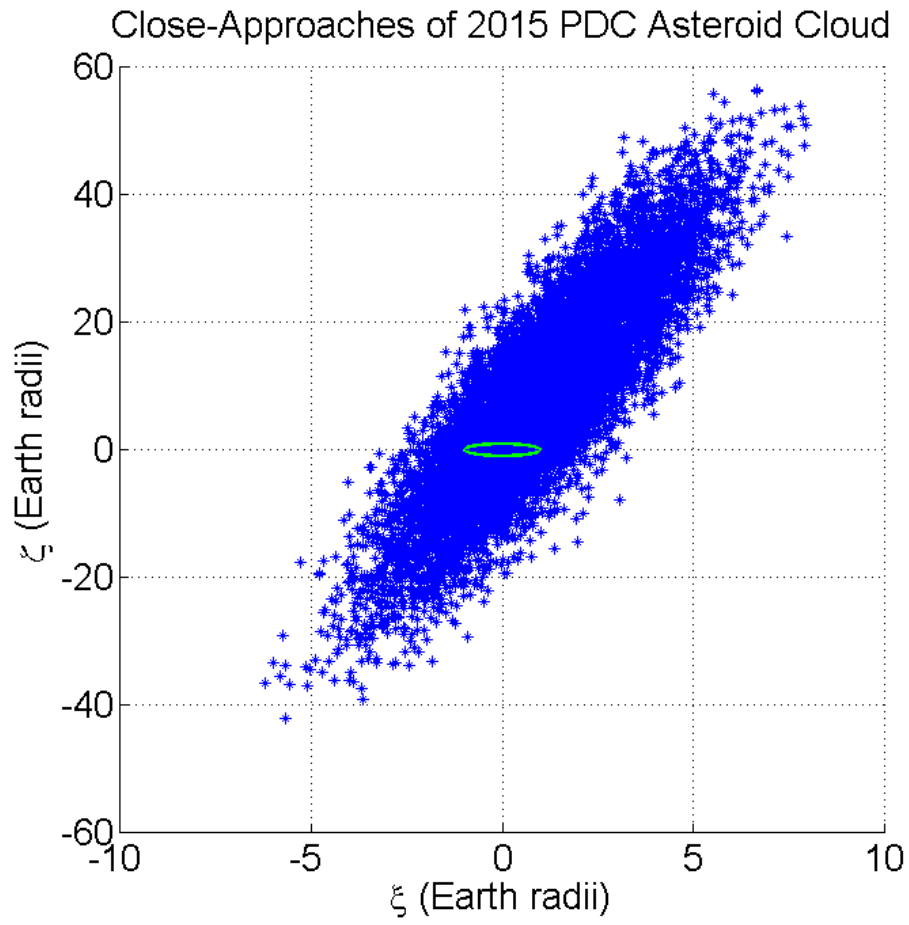
17

Figure 16: Asteroid 2015 PDC fragment cloud crossing locations on close-encounter B-plane.
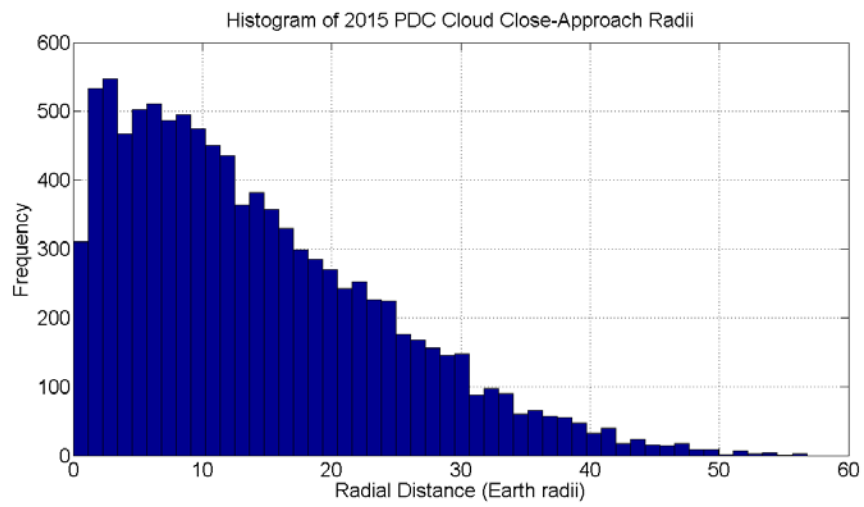

Figure 17: Histogram of asteroid 2015 PDC's fragment cloud radial crossing locations.
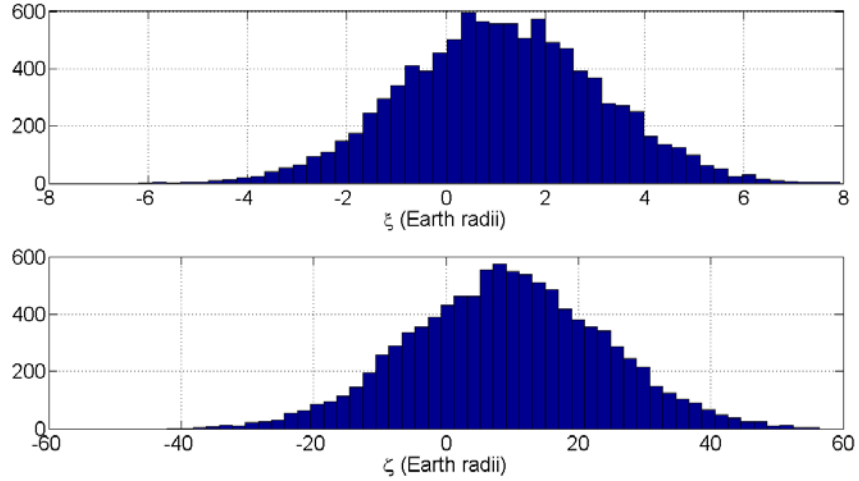
Figure 18: Top: Histogram of asteroid 2015 PDC's fragment cloud ξ components. Bottom: Histogram of asteroid 2015 PDC's fragment cloud ζ components.

ζ-component however, appears to be comprised of two different normal distributions (one for the left portion of the distribution and one for the right portion).

Switching focus back to the current and future risk posed by the asteroid fragment to the Earth, Figure 19 is used to better understand the future risk imposed by the chosen fragment. The plot shows three potential resonances that the asteroid fragment could fall into given its encounter with the Earth and the crossing location of the fragment's nominal trajectory, with respect to the cross-section of the Earth on the B-plane. However, this fragment's post-encounter trajectory does not fall into one of those resonance orbits. The calculated, expected crossing position of the asteroid fragment on the next encounter B-plane is at a ξ-value of about 120 Earth radii from the center of the Earth, nowhere near the small resonance circles. According to analytic keyhole theory, the resonances represented by the blue resonance circles have no keyholes on the depicted 2022 B-plane, due to there being no intersections between the resonance circles and the expected ξ-value line on the future encounter. Just because this fragment does not present a risk to the Earth in the near future, does not mean that the threat from this fragment is non-existent. There could be potential dangers to the Earth that go beyond the 10 year future that was looked at in this analysis. A different methodology must be used to adequately evaluate those future potential risks because of the length of time between the encounters and the perturbations that could sufficiently effect the orbit over that timespan.

Even though there has been an assessment of the likelihood of the fragment from asteroid 2015 PDC impacting the planet on its 2022 encounter, the keyhole passage probability equation (Equation 15) can be used to find another estimate for the impact probability. For this particular fragment cloud, all 10,001 simulated virtual fragments had an encounter with the planet, which makes $p_{encounter}$ equal to one. Instead of putting a bounding box around the simulated crossing locations an ellipse would fit the distribution better, leaving a smaller proportion of the data outside of the bounding area while including less extraneous areas of the B-plane. Compiling the appropriate values and plugging them into the formula, the resulting impact probability comes to be about 0.011% - about two orders of magnitude smaller than the numbers listed previously. The reason for the discrepancy can attributed to a number of reasons: (1) the value obtained from Equation (15) is made assuming that the crossing locations on the B-plane are evenly distributed throughout the bounded areas used in the calculations, (2) the estimated impact probability calculated from the fitted distribution is dependent on how well the distribution fits the data, and (3) the calculated impact probability using the number of simulated virtual impacts and virtual asteroid fragments is dependent on the number of simulated asteroid fragments, where the resulting impact probability should approach the true value as the number of values increases. What can be done with the various impact probabilities from the fragment cloud is that they can be used as bounds for what the true impact probability would be for the asteroid.

Looking back at Figure 15, it seems that the Earth is sitting in a region of the B-plane map where there is a non-negligible chance of it getting hit by more than one asteroid fragment, given the modeled fragmentation event. If it is assumed that the fragmentation only produces the 10001 asteroid fragments simulated in this example, only about 5,200 of the 10,001 virtual asteroid fragments ended up having an immediate encounter with Earth, and only 15 of those passed with 1.1 Earth radii of the planet center. What that means is that given this type fragmentation event, with a year timespan for the asteroid fragments to disperse from the original asteroid's impact trajectory, the Earth would only be impacted with about 0.15% of the total asteroid mass, rather than the full asteroid mass if
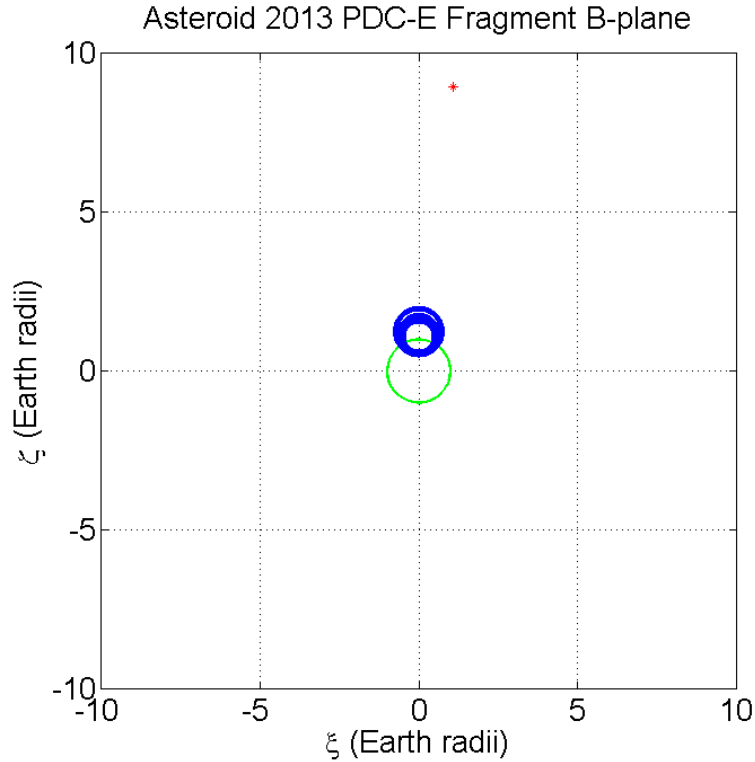
19

Asteroid 2013 PDC-E Fragment B-plane

Figure 19: Depiction of asteroid 2015 PDC's fragment resonance circles. The black vertical lines depict the corridor where the fragment's crossing location on the next encounter B-plane. The red star depicts the fragment's crossing location on the current encounter B-plane.

nothing were done to deflect/disrupt the target body. And, if the assumption is made that the mass of the asteroid is evenly distributed among the simulated asteroid fragments, the 15 impacting virtual asteroid fragments would only cause localized damage to the parts of the Earth they impact (if they make landfall), rather than the potential regional or global damage that could be caused by the full asteroid impacting the planet.

6. Conclusions

The threat of a fictional asteroid 2015 PDC, which is discovered about seven years prior to its expected impact date, has been discussed. The process of analyzing the impact risk of this asteroid and designing rendezvous and disruption missions has also been discussed, with an emphasis on the current and future risk posed by a disruption mission. Given nothing but the initial asteroid state at a given epoch, an asteroid cloud was constructed using assumed orbital uncertainties based on orbital uncertainties similar to those of similar near-Earth asteroids. Not surprisingly, as the orbital uncertainty decreased, the impact risk grew. After analyzing the asteroid fragment cloud, a representative fragment was selected to be analyzed in terms of its potential resonance orbits, keyhole existence on the encounter B-plane, and the likelihood of passing through those keyholes. The selected asteroid fragment has three very small possible resonance circles it could fall in, but the encounters on those future B-planes occur more than 100 Earth radii away from the Earth, meaning that there is no resonance or keyhole passage potential. The possibility of that fragment impacting the Earth is non-negligible. Overall, asteroid 2015 PDC is regularly accessible from Earth for deflection/disruption missions, difficult to rendezvous with due to the shape and orientation of the orbit, has a fairly high impact risk if unabated, and if fragmented a year prior to its expected impact, the risk to Earth is less due to the amount of fragments that would come near the Earth and the amount of mass that would encounter the planet.

References

[1] http://neo.jpl.nasa.gov/pdc15/
[2] Pitz, A., Kaplinger, B., Vardaxis, G., Winkler, T., and Wie, B., "Conceptual Design of a Hypervelocity Asteroid Intercept Vehicle (HAIV) and Its Flight Validation Mission," *Acta Astronautica* 94 (2014) 42-56.
[3] Barbee, B., Wie, B., Mark, S., and Getzandanner, K., "Conceptual Design of a Flight Demonstration Mission for a Hypervelocity Asteroid Intercept Vehicle," *Acta Astronautica*, Vol. 106, 2015, pp. 139-159.

[4] Vardaxis, G. and Wie, B., "Near-Earth Object Intercept Trajectory Design for Planetary Defense," *Acta Astronautica* Vol. 101, Aug-Sept, 2014, pp. 1-15.

[5] "Effects of Nuclear Earth- Penetrators and Other Weapons." National Research Council, The National Academies Press, 2005.

[6] Wie, B. and Barbee, B. "An Innovative Solution to NASA's NEO Impact Threat Mitigation Grand Challenge and Flight Validation Mission Architecture Development," Final Report of a NASA Innovative Advanced Concepts Phase 2 Study, December 2014.

[7] NASA JSC Cost Estimating and Models. Advanced Missions Cost Model. 2007.

[8] Wagner, S., Wie, B., and Barbee, B., "Target Selection for a Hypervelocity Asteroid Intercept Vehicle Flight Validation Mission," *Acta Astronautica*, Vol. 107, 2015, pp. 247-261.

[9] Chodas, P. W. and Yeomans, D., "Orbit Determination and Estimation of Impact Probability for Near Earth Objects," AAS 09-002, *AAS/AIAA Space Flight Mechanics Meeting, 2009.*

[10] Yeomans, D. K., Chodas, P. W., Sitarski, G., Szutowicz, S., and Krolikowska, M., "Cometary Orbit Determination and Nongravitational Forces," Comets II, The Lunar and Planetary Institute, 2004, pp. 137-152.

[11] Sharaf, M.A. and Selim, H.H., "Final State Predictions for J2 Gravity Perturbed Motion of the Earth's Artificial Satellites Using Bispherical Coordinates," NRIAG Journal of Astronomy and Geophysics (2013) 2, 134-138.

[12] Carusi, A., Valsecchi, G. B., and Greenberg, R., "Planetary Close Encounters: Geometry of Approach and Post-Encounter Orbital Parameters," *Celestial Mechanics and Dynamical Astronomy*, Vol. 49, 1990, pp. 111-131.

[13] "Gravity Assist Interplanetary Trajectories." *Welcome to the Orbital and Celestial Mechanics Website,* C. David Eagle, 9 Dec. 2012. Web. 4 Dec. 2013.

[14] Milani, A., Chesley, S. R., Chodas, P. W., and Valsecchi, G. B., "Asteroid Close Approaches: Analysis and Potential Impact Detection," Asteroids III, The Lunar and Planetary Institute, p. 55-69, 2002.

[15] Valsecchi, G. B., Milani, A., Chodas, P. W., and Chesley, S. R., "Resonant Returns to Close Approaches: Analytic Theory," *Astron. Astrophys.*, 2001.

[16] Pitz, A., Teubert, C., and Wie, B., "Earth-Impact Probability Computation of Disrupted Asteroid Fragments Using GMAT/STK/CODES," AAS 11-408, AAS/AIAA Astrodynamics Specialist Conference, Girdwood, AK, August 1-4, 2011.

[17] Vardaxis, G., and Wie, B., "Impact Risk Assessment for a Fragmented Asteroid in Earth Resonant Orbits, AIAA-2014-4300, AIAA/AAS Astrodynamics Specialist Conference, San Diego, CA, August 4-7, 2014.

[18] Battin, R. "An Introduction to the Mathematics and Methods of Astrodynamics, Revised Edition." Ch. 7: Solving Lambert's Problem, AIAA Education Series, 1801 Alexander Bell Drive, Reston, VA, 1999.

[19] Born, G. H. Design of the Approach Trajectory: B-plane Targeting. University of Colorado Boulder: ASEN 5519-Interplanetary Mission Design, 2005.

[20] "Near-Earth Object Survey and Deflection Study Report," NASA, 2006.

[21] "Defending Planet Earth: Near-Earth Object Surveys and Hazard Mitigation Strategies," Report No. 0-309-14968-1, National Research Council, National Academy of Sciences, 2010.